

(accepted for publication in Medical & Biological Engineering & Computing)

A Coupled Flow-Acoustic Computational Study of Bruits from a Modeled Stenosed Artery

Jung Hee Seo, Rajat Mittal

*Department of Mechanical Engineering, Johns Hopkins University,
Baltimore, MD, 21218*

Corresponding Author:

Rajat Mittal

e-mail: mittal@jhu.edu

Phone: +1-410-516-4069

Fax: +1-410-516-7254

Abstract

The sound generated by blood flow in stenosed arteries is investigated for a model that consists of a channel with a one-sided constriction. The blood flow-induced arterial “bruits” are computed directly using a hybrid approach wherein the hemodynamic flow field is solved by an immersed boundary, incompressible flow solver, and the sound generation is modeled by a first-principles approach that employs the linearized compressible perturbation equations. The transmission and propagation of the sound through the surrounding biological tissues is also modeled with a simplified, linear structural wave equation. The flow field inside the artery and the bruit sound signal at the epidermal surface are examined to delineate the precise source of the arterial bruit and the correlation between the bruit and the arterial wall pressure fluctuations. It is found that the bruits are related primarily to the time-derivative of the integrated pressure force on the post-stenotic segment of arterial wall. The current study provides a clear perspective on the generation of bruits from stenosed arteries and enables an assessment of the conjectures of previous researchers regarding the source of arterial bruits.

Keywords: Stenosis, Artery, Murmur, Hemoacoustics, Immersed Boundary Method

Introduction

An arterial stenosis is an abnormal narrowing in a artery which is normally caused by atherosclerosis. It is often found in the coronary, carotid, and femoral arteries, and presents severe health risks to the patient[4,29]. The diagnosis of arterial stenoses can be made with ultrasound, MRI (Magnetic Resonance Imaging), or MRA (Magnetic Resonance Angiogram), but these methods are time-consuming, expensive, and often invasive. Meanwhile, it is well established that stenosed arteries produce distinct sounds known as arterial *bruits* (or *murmurs*) which can be heard externally with a stethoscope. This technique of “auscultation” is a non-invasive, inexpensive and safe diagnostic method for arterial stenosis[4,34].

Although it has been generally believed that arterial bruits are associated with the “disturbances” in the blood flow caused by the stenosis, the precise source mechanism of the bruit is still poorly understood. Bruns[9] argued that arterial bruits were generated by the ‘*nearly periodic fluctuation in the wake found downstream of any appropriate obstacle*’ and not by post-stenotic turbulence which is a quadruple sound generation mechanism with exceedingly low strength at low Mach numbers. Lees and Dewey[21] recorded the spectrum of actual bruit sounds (a technique called *phonoangiography*), and suggested a significant similarity between the bruit sound spectrum and the wall pressure spectrum of a fully developed turbulent pipe flow which seemed to contradict the postulate of Bruns. Fredberg[12] derived a theoretical model for the transfer function between wall pressure spectrum and sensed sound using the Green’s function and a stochastic analysis of turbulent boundary layer. Wang et al.[39] modeled the sound generation in a stenosed coronary artery using an electrical network analog model, and Borisyuk[7] modeled the sound propagation through the tissues (thorax) theoretically for a simple cylindrical geometry. It should be noted that both Wang et al. and Borisyuk use an empirical turbulence spectrum as an input to the sound analysis. Borisyuk[8] also conducted an experimental study for the sound generation by steady flow through a stenosed duct with a thorax model and analyzed the sound spectra. Yazicioglu et al.[40] performed an experiment for the flow inside a constricted viscoelastic tube that was ensconced in a gel phantom model, and measured the tube wall pressure as well as the surface vibration of the

gel phantom Interestingly, Owsley and Hull [31] conducted a similar study but focused on the propagation of shear waves.

In addition to these, there have been many numerical and experimental studies of the flow field and turbulence characteristics of blood flow in stenosed arteries including those of Fredberg[13], Kirkeeide et al.[19], Ahmed & Giddens[1,2], Mittal et al.[24], and Varghese et al.[37,38]. Most of studies on stenotic flows associated with arterial bruit have focused on the arterial wall pressure fluctuations as a surrogate for sound[13,18,24] or as a dominant source for the arterial bruit[7,12,39]. The correlation between the bruit sound and the arterial wall pressure however remains to be established.

The objective of the present study is to investigate the source mechanism of arterial bruits and the correlation between bruits and the arterial wall pressure fluctuation via a physics-based, coupled flow-acoustic computational model. The direct simulation of blood-flow induced sound is challenging, since the flow Mach number is very low and wave propagation through different materials is also involved. In this study, the problem is tackled with an immersed-boundary method based hybrid approach, and we simulate blood flows as well as the sound generation and propagation for a canonical model of a stenosed artery.

Methods

At the outset, we point out that the major assumptions made in the current computational model are that the blood behaves like a Newtonian fluid, the wall of the blood vessel is not deformed by the blood-flow, the shear waves generated in the tissue are negligible compares to the acoustic waves and that the viscous dissipation of the acoustic wave is also negligible. Justifications for these assumptions is provided in the following section.

Model

A two-dimensional constricted channel is considered as a model of a stenosed artery and a schematic is shown in Fig. 1. A channel is constricted from one side (top wall) and the profile of constriction is given by

$$y = y_{\max} - \frac{b}{2} \left[1 + \cos \left(2\pi \frac{x - x_0}{D} \right) \right], \quad -D \leq (x - x_0) \leq D \quad (1)$$

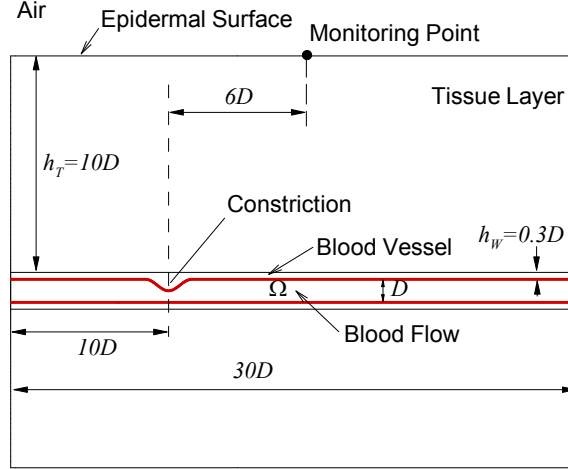


Figure 1. Schematic of the constricted channel model and acoustic domain; D : arterial diameter, h_w : arterial wall thickness, h_T : tissue layer thickness.

where b is the size of constriction, x_0 is the center of the stenosis, and D is the height of the channel. Similar models have been used in past studies of constricted arteries [1,2,37,38]. Two constriction levels corresponding to $b=0.5D$ and $0.75D$ are considered in the present study. The pulsatile pressure drop between the inlet and exit is assumed to have the following sinusoidal variation in time:

$$\Delta P / \rho U^2 = A + B \cdot \sin(2\pi ft), \quad (2)$$

where constants A and B are chosen to obtain similar maximum flow rate for two cases (50% and 75% constrictions) and a minimum flow rate close to zero. Thus, B is fixed to 1.5, while value A is set to 0.225 and 0.75 for the 50% and 75% cases, respectively. The non-dimensional frequency of pulsation is $St=fD/U_{max}=0.024$, where U_{max} is the maximum centerline velocity at the inlet, and the Reynolds number is set to $Re=U_{max}D/\nu_0=2000$, where ν_0 is a kinematic viscosity. The chosen flow parameters yield a Womersley number[29], $\alpha = (\pi \cdot Re \cdot St / 2)^{1/2} = 8.6$ which is in the range appropriate for large peripheral arteries[24].

In the current model, the blood flow is assumed to be Newtonian (which is a good assumption for the larger and medium sized arteries[32]) and the fluid-structure interaction with the arterial wall is neglected. Fluid-structure interaction with the elastic blood vessel may introduce resonance peaks in the sound spectrum[23]. However, these resonance peaks are generally diminished due to

the damping associated with the surrounding tissue[23] and do not play an important role in auscultation.

The acoustic domain in the current study includes not only the lumen but also the arterial wall (blood vessel) and the surrounding tissue (assumed to be skin). The acoustic material properties are based on Ref. [16]; the density and speed of sound for the blood, vessel wall and tissue are 1.05 (g/cm³) and 1500 (m/s), 1.1 (g/cm³) and 1580 (m/s), and 1.2 (g/cm³) and 1720 (m/s), respectively. The top boundary of the acoustic domain represents the epidermal surface and given that a stethoscope actually senses transmitted sound via the velocity (or acceleration) of the epidermis[7], we monitor these quantities in our simulations. It is assumed that the acoustic waves radiate through all other boundaries.

Hemodynamics

The hemodynamic flow field inside the artery is modeled with an immersed boundary solver[25] which solves the following incompressible Navier-Stokes equations,

$$\frac{\partial \vec{U}}{\partial t} + (\vec{U} \cdot \nabla) \vec{U} + \frac{\nabla P}{\rho_0} = \nu_0 \nabla^2 \vec{U}, \quad \nabla \cdot \vec{U} = 0, \quad (3)$$

where \vec{U} is velocity vector, P is pressure, and ρ_0 is the density of blood. In this study, the equations are solved by a projection method with a second-order central finite-difference scheme and a ghost-cell based sharp-interface method is used for the immersed boundary treatment. The details of the flow solver and the immersed boundary formulation can be found in Ref. [25].

The blood flow domain is resolved by a 768×128 non-uniform Cartesian grid with the minimum grid spacing $\Delta x=0.01D$. The flow is driven by the pulsatile pressure gradient and Dirichlet pressure boundary conditions are applied at the inlet and exit. A Neumann type boundary condition is applied for the velocity at the inlet and exit, and a no-slip boundary condition is used for the top and bottom walls. The flow computations are carried out for about 4 pulsation cycles after it reaches a stationary state.

Acoustics

The flow-induced sound in the blood flow region is computed by the linearized perturbed compressible equations (LPCE)[35] which are given by

$$\begin{aligned}\frac{\partial \bar{u}'}{\partial t} + \nabla(\bar{u}' \cdot \bar{U}) + \frac{1}{\rho_0} \nabla p' &= 0, \\ \frac{\partial p'}{\partial t} + (\bar{U} \cdot \nabla) p' + \rho_0 c_0^2 (\nabla \cdot \bar{u}') + (\bar{u}' \cdot \nabla) P &= -\frac{DP}{Dt},\end{aligned}\quad (4)$$

where the (') represents the compressible (acoustic) perturbation, c_0 is the speed of sound, and D/Dt is the total derivative. The capital letters indicates the hydrodynamic incompressible variables and they are obtained from the incompressible flow simulations. The details of the derivation and the validation of the above procedure can be found in Ref.[35]. The incompressible Navier-Stokes/LPCE hybrid method is a two-step, one-way coupled approach for the prediction of flow induced sound at low Mach numbers[26,35,36].

The auscultated sound is in fact the sound signal monitored on the skin (epidermal) surface. The propagation of the sound through the tissues between the artery and the epidermal surface is therefore an important aspect of modeling arterial bruits[5,7,12]. In the present study, the sound propagation through the arterial wall and surrounding tissue is modeled via a linear structural wave equation based on the bulk modulus of the tissue material as follows:

$$\begin{aligned}\frac{\partial \bar{u}'}{\partial t} + \frac{1}{\rho_s} \nabla p' &= 0, \\ \frac{\partial p'}{\partial t} + K(\nabla \cdot \bar{u}') &= 0,\end{aligned}\quad (5)$$

where \bar{u}' is the velocity fluctuation vector (time derivative of displacement) and p' represents the average normal stress (pressure), and ρ_s and $K=\rho_s c_s^2$ are the density and the bulk modulus of the material, respectively. In this model the propagation of shear waves is not considered; this approach is valid since the shear modulus of the tissue materials is much smaller than the bulk modulus[30]. Also shear wave length is much shorter than the compression wave and thus it decays rapidly. This fluid-like assumption of the tissue material for the purpose of resolving acoustic wave propagation has been widely used for the simulation of ultrasound[6,30] and acoustic[28] wave radiation in biological materials. Previous analytical studies[7,12] on arterial bruits also focused on the propagation of compression waves. The dissipation of the acoustic wave is also neglected in the

present study since the frequency range of the bruits is typically on the lower end of the spectrum (<1000 Hz) and the dissipation of acoustic wave at these low frequencies is expected to be very small[12]. Specifically, the attenuation loss coefficient for tissue is about 0.1(neper·MHz/cm)[15] and this yields only about a 0.01% loss at 1000 Hz.

Equation (5) is solved in a fully coupled manner with the LPCE. In fact, in the present study, we combine those two into a single set of equations and the different material domains are treated by prescribing appropriate material properties. The following unified single set of acoustic equations result from this combination:

$$\begin{aligned} \frac{\partial \vec{u}'}{\partial t} + H(\vec{x})\nabla(\vec{u}' \cdot \vec{U}) + \frac{1}{\rho(\vec{x})}\nabla p' &= 0, \\ \frac{\partial p'}{\partial t} + H(\vec{x})\left[(\vec{U} \cdot \nabla)p' + (\vec{u}' \cdot \nabla)P\right] + K(\vec{x})(\nabla \cdot \vec{u}') &= -\frac{DP}{Dt}H(\vec{x}), \end{aligned} \quad (6)$$

where H is a Heaviside function of which values is 1 for the blood flow region and 0 for elsewhere, and the density (ρ) and bulk modulus ($K=\rho c^2$) are now functions of space. By solving Eqs. (6), the wave transmission and reflection at the interface between the blood and tissue are automatically resolved based on the difference of acoustic impedance $Z=K/c$. The same approach has been used in the simulations of sound wave propagation through heterogeneous materials[6,28]. Equations (6) are spatially discretized with a sixth-order compact finite difference scheme[22] and integrated in time using a four-stage Runge-Kutta method.

The actual Mach number of blood flows in arteries is $M=U/c \sim O(10^{-3})$, where c is the speed of sound. This extremely low Mach number significantly increases the computational cost of the acoustic field simulation, because the time-step size is restricted by the speed of sound, which is much faster than the flow speed. In order to mitigate this computational expense, we employ a Mach number of 0.01. This may result in an increase in the absolute sound intensity, however, the source mechanism and the scaling between sound and pressure are unaffected, and comparisons between different cases and different source locations can still be made. It should be noted that even with this increased Mach number, the acoustic (compression) wave length of the bruit remains much larger than any other length scale in the problem. A similar, $O(10)$ increase of Mach number (decrease of speed of sound) was also used in the previous study of Eienstein et al.[11] for the computation of mitral-valve sound in the heart.

The acoustic domain is covered by a 400×200 Cartesian grid with a minimum grid spacing 0.02*D*. The acoustic wave length is about 20*D* for the frequency of St=5, and this wave length is resolved by about 200 grid points. At the epidermal surface, a zero-stress boundary condition ($p'=0$) is applied [5,7]. A buffer-zone type radiation boundary condition is applied via grid stretching and low-pass spatial filtering[14] at all the other boundaries. The flow simulation results are interpolated onto the acoustic grid in the lumen using a bi-linear interpolation. The time-step for the acoustic field simulation is 20 times smaller than the time-step size used for the incompressible flow simulation due to the acoustic CFL condition, and a second-order Lagrangian interpolation[36] is used for the temporal interpolation of flow variables.

Analytical Evaluation of Sound Source

The source of the bruit is evaluated analytically for the present model configuration to aid the investigation of the source mechanism. The wave equation for the acoustic velocity fluctuation in the absence of shear waves can be written as

$$\frac{\partial^2 \vec{v}'}{\partial t^2} + c_s^2 \nabla^2 \vec{v}' = \frac{1}{\rho_s} \frac{\partial \vec{f}}{\partial t}, \quad (7)$$

where c_s is the speed of sound obtained from the bulk modulus as $c_s = \sqrt{K/\rho_s}$, and \vec{f} is the external body force per unit volume. In the analytical model, the inhomogeneity of material properties is not taken into account, since the differences in the values are quite small. The general solution of Eq. (7) can be obtained using the Green's function[17] as

$$\vec{v}' = -\frac{1}{\rho_s c_s^2} \int_{-\infty}^{\infty} \frac{1}{4\pi |\vec{r}|} \left[\frac{\partial \vec{f}}{\partial t} \right]_{\tau} dV, \quad (8)$$

where \vec{r} is the vector from the source to the observer point, and the square-bracket indicates the value evaluated at the retarded time, $\tau = t - |\vec{r}|/c_s$. For the present configuration, the external force is exerted by the blood flow and is associated with the fluid pressure. The force term in Eq. (8), therefore, can be replaced by the pressure gradient;

$$\bar{v}' = \frac{1}{4\pi\rho_s c_s^2} \int_{-\infty}^{\infty} \frac{1}{|\bar{r}|} \left[\frac{\partial}{\partial t} \nabla(PH) \right]_{\bar{r}} dV, \quad (9)$$

where H is a Heaviside function for which the value is 1 inside the blood flow domain and 0 otherwise. Integration by parts of Eq. (9) leads to

$$\bar{v}' = -\frac{1}{4\pi\rho_s c_s^2} \int_{\Omega} \frac{\bar{r}}{|\bar{r}|^3} \left[\frac{\partial P}{\partial t} \right]_{\bar{r}} dV. \quad (10)$$

The volume integration is therefore reduced to the blood flow domain which is denoted by Ω in Fig.1. If we now assume that the pressure on the upper and the lower surfaces of the lumen are not significantly different, Eq. (10) can be approximated by the trapezoidal rule for the y -component of velocity fluctuation on the epidermal surface as

$$v' \approx -\frac{D}{2\pi\rho_s c_s^2} \int_0^{L_z} \int_0^{L_x} \frac{\sin\theta}{r^2} \left[\frac{\partial P}{\partial t} \right]_{\bar{r}} dx dz, \quad (11)$$

where θ is the angle between the x -axis and \bar{r} . Here x and z are the axial and spanwise directions of the channel, respectively, and y is the direction towards the epidermal surface. Furthermore, L_x and L_z are the streamwise and spanwise lengths of the blood flow region, and $r = |\bar{r}|$. The boundary condition on the epidermal surface ($\partial v' / \partial y = 0$, with a zero stress boundary condition) is also applied on the Eq. (11) by means of an anti-symmetric imaginary source. If it is assumed that $r \approx r_a = \text{const.}$, where r_a is the average distance, and $\theta \approx \pi/2$, the above expression can be further simplified to;

$$v' \approx -\frac{D}{2\pi\rho_s c_s^2 r_a^2} \left[\frac{dF_y}{dt} \right]_{\bar{r}}; \quad F_y = \int_0^{L_z} \int_0^{L_x} P dx dz, \quad (12)$$

where F_y is the pressure force integrated on the upper(or lower) boundary surface of the blood flow domain. Note that the above equation is the result for three-dimensional wave radiation. For a two-dimensional case, the equivalent form of Eq. (12) is written in the frequency domain as

$$\hat{v}'(\omega) \approx -\frac{iDk}{2\rho_s c_s^2} H_1^{(1)}(kr_a) \cdot \widehat{\frac{dF_{y,2D}}{dt}}(\omega); \quad F_{y,2D} = \int_0^{L_x} P dx, \quad (13)$$

where $k = \omega/c_s$ is the wave number, H_1 is the Hankel function of order 1, and hat (^) indicates a Fourier transform. The time signal may be given by

$v'(t) = \int_{-\infty}^{\infty} \hat{v}'(\omega) e^{-i\omega t} d\omega$. The analytical expression derived here suggests that the vertical velocity fluctuation detected by a stethoscope is generated by the time-derivative of the integrated pressure force, F_y . This theoretical estimate can be examined using the current computational model.

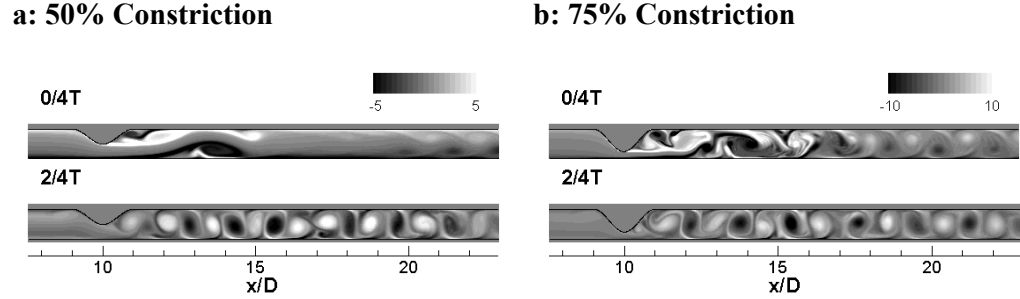


Figure 2. Time evolution of vorticity field; 0/4T: maximum flow rate, and 2/4T: minimum flow rate phase.

Results

Hemodynamics

Unless otherwise noted, all the data presented in this paper are non-dimensionalized by the velocity scale: U_{\max} , length-scale: D , time-scale: D/U_{\max} , and pressure scale: ρU_{\max}^2 . The instantaneous hemodynamic flow fields are visualized in Fig. 2 by contours of spanwise vorticity. For the 50% constriction case (Fig. 2a), it is observed that the vortex roll-up starts from the maximum flow rate phase (0/4T, where T is the period of pulsation). The detachment of separation bubble in the wake of the stenosis, and the boundary layer separation at the bottom surface are clearly visible. The shear layers become unstable during deceleration and a coherent vortex street is formed as shown at 2/4T with an overall wavelength of about $\sim 1D$. For the 75% case (Fig. 2b), more complex and stronger (see the contour legend) vortex motions are observed. The separation bubble in the wake of the stenosis rapidly becomes unstable, and a strong, jet-like flow through the gap below the constriction induces large-scale vortex roll-up (of which length scale $\sim 1D$) as well as the formation of smaller-scale vortices. At the minimum flow rate and beyond, a vortex street similar to the 50% constriction

case is observed and for both cases, a clear signature of the vortex street persists into the next cycle. The overall flow patterns are similar to the 3D large-eddy simulation (LES) results of Mittal et al.[24]. However, in 3D LES, the large vortex structures break into smaller eddies in the post-stenotic region reducing the coherence of the vortex street.

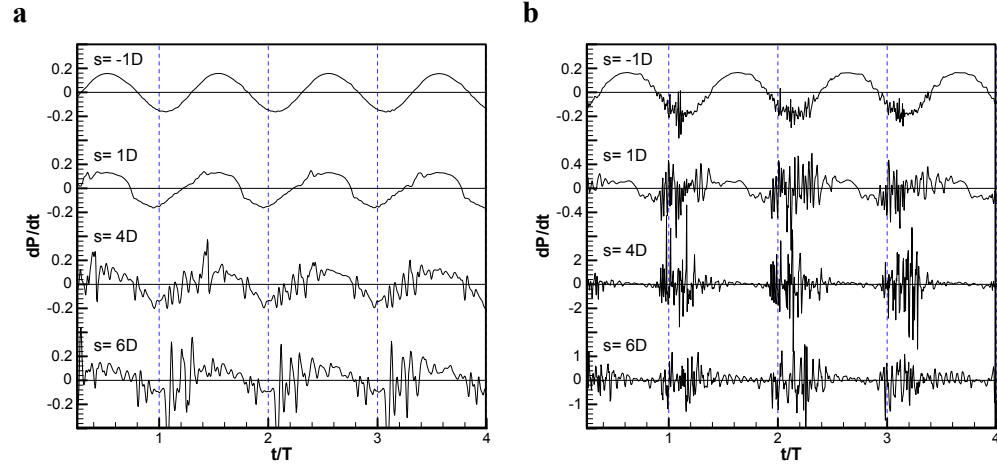


Figure 3. Time variations of temporal wall pressure fluctuation represented by the time derivative of pressure at several locations on the upper lumen, where $s=(x-x_0)$ is the distance from the center of the stenosis and T is the period of pulsation. a) 50% constriction case, b) 75% case. Vertical dashed lines indicate the maximum flow rate phase.

The temporal wall pressure fluctuations represented by the time-derivatives of pressure, dP/dt are monitored at the following locations on the upper wall; $1D$ upstream from the center of stenosis (begin of the constriction), and $1D$ (end of the constriction), $4D$, and $6D$ downstream from the center of the stenosis, and plotted in Fig. 3. The last two downstream locations correspond to the position of the maximum pressure fluctuation for 75% and 50% constriction cases, respectively. For the 50% case, the temporal pressure fluctuation is found to be the superposition of the overall pulsation of pressure gradient and the fluctuations caused by the post-stenotic vortex motion. For the 75% case, the magnitude of the pressure fluctuation induced by the vortex motion is about 10 times larger than the 50% case, especially at $4D$ downstream from the stenosis, and the most severe pressure fluctuations are observed at around the maximum flow rate phase.

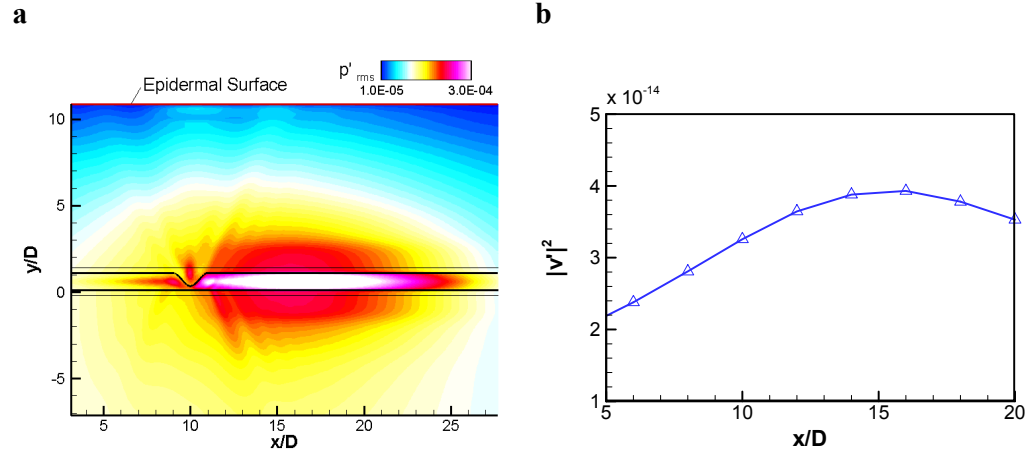


Figure 4. a) Root mean squared acoustic pressure fluctuation (p'_{rms}) for 75% constriction case. b) Intensity of vertical velocity fluctuation on the epidermal surface.

Arterial Bruits

The root-mean-squared (rms) acoustic pressure fluctuation field is shown in Fig. 4a for 75% constriction case. In this plot, the origin of the acoustic waves seems to be at the post-stenotic region. The vertical velocity fluctuation on the epidermal surface which represents the arterial bruit is monitored at a number of positions and the stream wise variation of the intensity is plotted in Fig. 4b. The bruit is strongest over the post-stenotic region and a shallow peak is observed at 5-6D downstream from the stenosis which is consistent with Fig. 4a. However, finding that the spectral characteristics at different locations are nearly indistinguishable, we analyze the signal at one location: 6D downstream from the stenosis where the maximum acoustic energy is measured. The monitored time signals are plotted in Fig. 5a for two cases. Since some transducers sense acceleration which is proportional to the force or pressure, the epidermal acceleration (dv'/dt) is also shown. For the 50% constriction, small fluctuations are superimposed on the overall sinusoidal profile which is caused by the pressure gradient pulsation, but the amplitude of these fluctuations is relatively small. For the 75% case however, stronger high frequency fluctuations are observed, especially during the peak phase of the sinusoidal variation. This additional higher frequency fluctuation is expected to produce a distinct arterial murmur and this is more clearly represented in the acceleration signal.

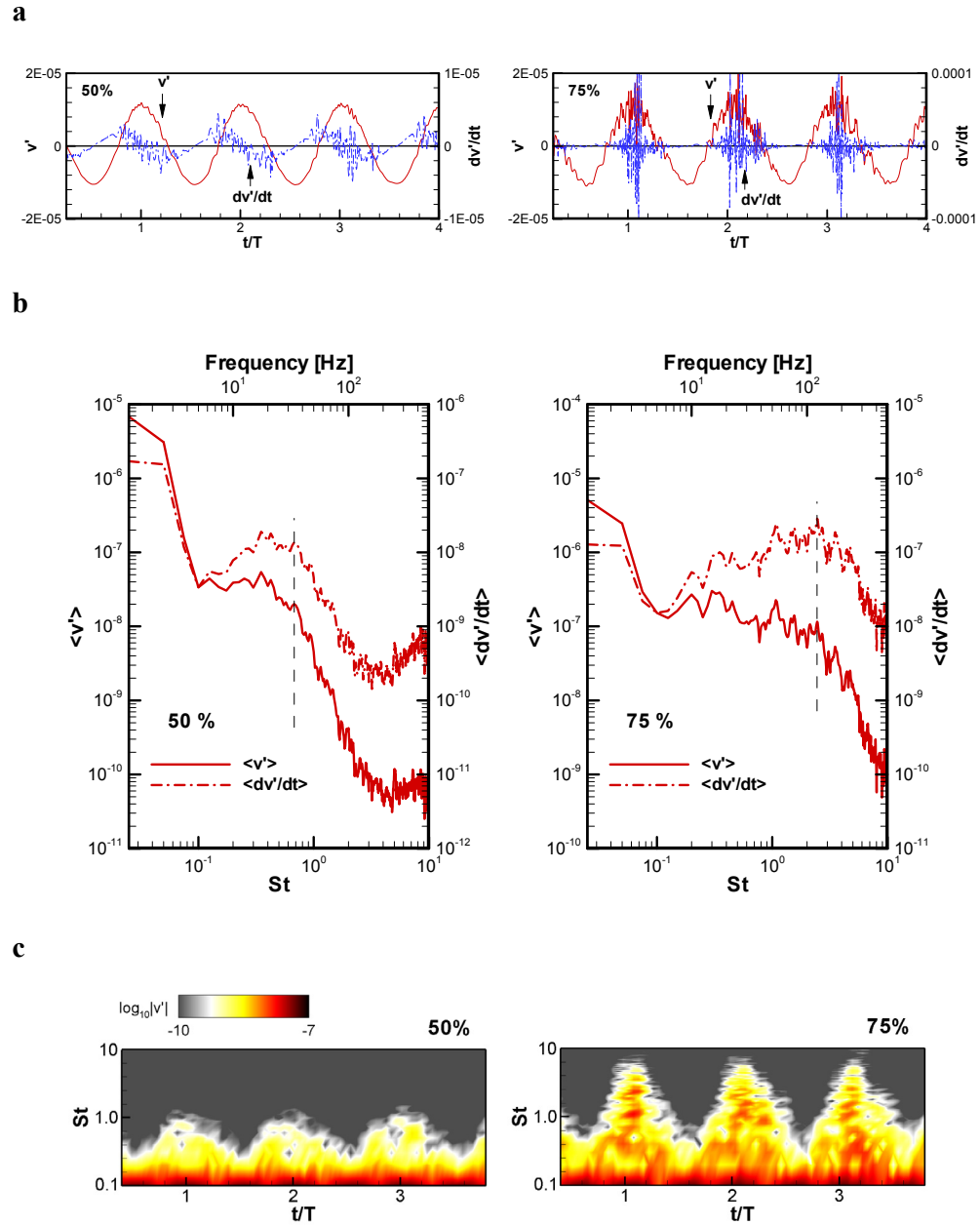


Figure 5. Vertical velocity fluctuations (v') and acceleration (dv'/dt) on the epidermal surface monitored $6D$ downstream from the center of the stenosis. a) Time series, b) frequency spectrum; Frequency in Hertz (Hz) is estimated by assuming the heart beat rate to be 75 BPM (beat-per-min). Vertical dashed lines indicate break-frequencies c) time-frequency spectrogram for $|v'|$.

The frequency spectra of v' and dv'/dt are shown in Fig. 5b. The peak at the origin represents the pulsation frequency ($St=0.024$) and this peak is followed by a broad-band spectrum for $St>0.1$, which represents the bruit. For 50% case, this broad-band spectrum is extends from $St=0.1$ to 1 but for the 75% case, the amplitude of the broad-band spectrum is significantly higher and the frequency

range extends up to $St \sim 5$. The vertical dashed lines indicate the break-frequency[10] where the slope of spectrum changes significantly, and the secondary peak is observed around the break-frequency in the acceleration spectrum. The bruit spectrum for the acceleration is very similar to the *in-vivo* measurement on the skin surface reported by Miller et al.[23]. Time-frequency spectrograms of epidermal velocity fluctuation computed by a short-term-Fourier transform[3] are also plotted in Fig. 5c for 50% and 75% cases and show the intensity and frequency content of the arterial bruit with respect to the phase of pulsation.

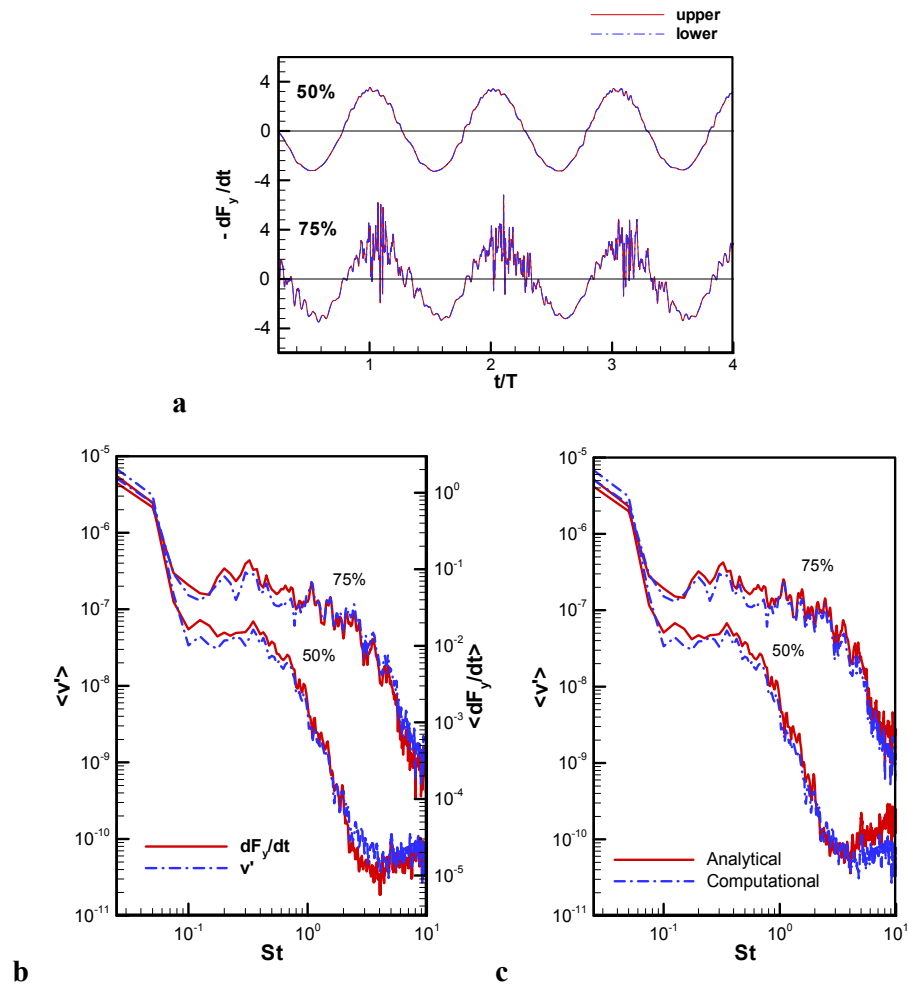


Figure 6. a) Time-derivative of pressure force integrated along the stream wise direction at the upper and lower surfaces of arterial wall. b) Comparison of bruit spectrum (v') and the spectrum of time-derivative of the integrated pressure force (dF_y/dt). c) The bruit spectrum as evaluated by Eq. (13). The spectrum is plotted along with the present computational result.

Sound Source

The integrated pressure force in the y -direction ($F_{y,2D}$ in Eq. 13, subscript 2D is dropped hereafter) is calculated for the upper and lower walls of the flow domain and its time derivative is plotted in Fig. 6a for the 50% and 75% cases. The pressure forces integrated on the upper and lower wall are almost identical and this supports our earlier assumption (used in deriving Eq. 13) that there is little difference between the upper and lower wall pressures. The computed frequency spectrum of the integrated pressure force is compared with the spectrum of velocity fluctuation at the epidermal surface in Fig 6b and found to match very well with the bruit spectrum for both cases. The bruit spectrum is also evaluated analytically using Eq. (13) and plotted along with the present computational result in Fig. 6c. Again, the two results agree very well not only for the shape but also for the amplitude.

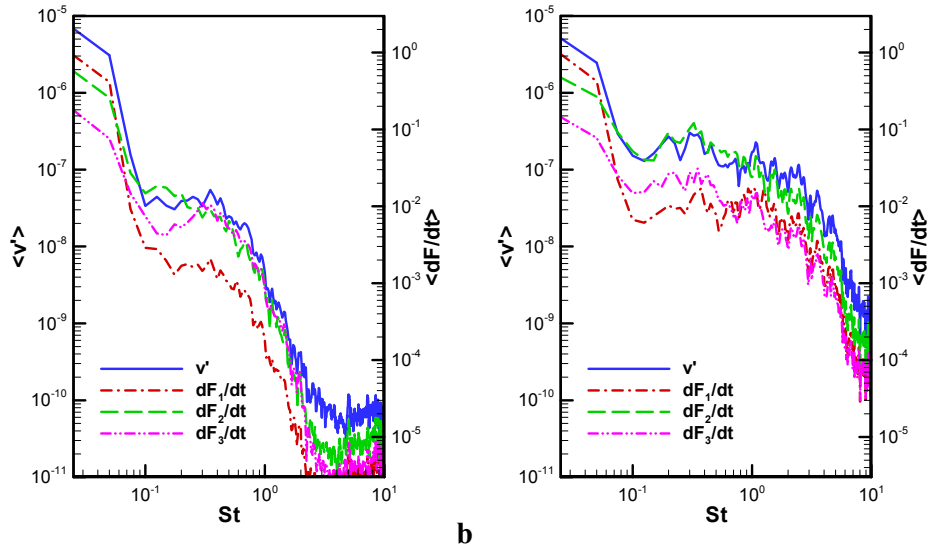


Figure 7. Comparison of bruit spectrum (v') and the spectrum of time-derivative of integrated pressure force for the segments of artery; F_1 : upstream region ($x/D=0\sim 10$), F_2 : post-stenotic region ($x/D=10\sim 20$), and F_3 : further downstream region ($x/D=20\sim 30$). a) 50% constriction and b) 75% constriction.

To find the region of the flow most responsible for the generation of source, the pressure integral in Eq. 13 is decomposed into three parts: i) the upstream region ($x/D=0\sim 10$), ii) near post-stenotic region ($x/D=10\sim 20$), and iii) far post-stenotic region ($x/D=20\sim 30$); these are denoted by F_1 , F_2 , and F_3 , respectively. The frequency spectra of the time-derivatives for each of the three force

components are plotted in Fig. 7 along with the bruit spectrum. For both the cases, the bruit spectrum for $St > 0.1$ coincides best with the spectrum of the force component from the near post-stenotic region ($x/D=10\sim 20$) which has an amplitude that is about an order-of-magnitude higher than that for the upstream component. For the 50% case, the force on the near and far post-stenotic region are comparable for higher frequencies ($St > 0.3$), while the force on the near post-stenotic region is dominant throughout the frequency range $St > 0.1$ for 75% case.

Discussion

In this study, an analysis of the computed results indicates that the epidermal velocity fluctuations are correlated well with the time-derivative of the pressure force on the lumen integrated over the near post-stenotic region. This supports the view that the primary source of arterial bruits is the vortex induced perturbations in the near post-stenotic region.

In the previous 3D LES study of Mittal et al.[24] which also employed a similar model, the maximum flow disturbance was found to be located near the flow re-attachment region where the shear layer rolls up and breaks up into vortices. In the present simulations, we also find that the shear layer breaks and rolls up into vortices around $4\sim 6D$ downstream from the stenosis, and the maximum wall pressure fluctuation is observed at these locations.

The present computations show that the acoustic fluctuation induced by the blood flow has a stronger intensity and higher frequency content for the higher level of constriction. This tendency is in line with the experimental observation of Borisyuk[8] and is mainly due to the fact that the jet velocity through the gap below the stenosis is higher for the larger constriction (smaller gap). The high frequency, high intensity components are important in auscultation, since they will make the bruit more audible to human ears. For both cases, however, the most energetic, high frequency components of the bruit are generated at (or near) the phase corresponding to the maximum flow rate. This observation is in line with the *in-vivo* study of Murgu[27] which addressed systolic ejection murmurs from heart. Note that while past computational hemodynamic [13,24] and experimental[19] studies have also found pressure fluctuations increasing with constriction severity and have constructed a similar connection between

constriction and bruit intensity, the current coupled flow-acoustic model proves this from first-principles.

The spectra, especially those corresponding to the epidermal acceleration, are very much inline with the general characteristics of arterial bruit described in Ref.[23]; the amplitude of spectrum slowly goes up to a discrete peak after which the intensity falls off rapidly with increasing frequency. The present epidermal acceleration spectrum shows good qualitative agreement with the *in-vivo* measurement of Miller et al.[23]. The “break-frequency”[10] which is a well-known characteristics of arterial bruits, is also observable in the present results. The break-frequencies estimated from the Fig. 5b are $St=0.68$ for the 50% case and $St=2.44$ for the 75% case. If the Strouhal number for the break frequency is computed as $St_2 = fd/u_j$, where d is the stenotic diameter ($d=D-b$, in the present study) and u_j is the volume averaged peak jet velocity through the stenosis[18], it yields $St_2 = 0.22$ and 0.20 the for 50% and 75% cases, respectively. The two values are not significantly different and therefore, the break frequencies identified here scale well with u_j and d . This observation also agrees with the experimental studies of Jones & Fronek[18] and the large-eddy simulation study of Mittal et al. [24]. It should be noted that the scaling of $St_2 \sim (d/D)^{0.26}$ suggested in Ref. [18] for a constricted pipe can be recast to $St_2 \sim (d/D)^{0.13}$ for the present 2D channel case, since the cross sectional area is linearly proportional to the diameter of channel, and the present results indicate a scaling of $St_2 \sim (d/D)^{0.138}$ which is commensurate with the above scaling.

The wall pressure fluctuations has long been believed to be responsible for the generation of arterial bruits[8,13,24]. In the previous study of Mittal et al.[24], the strongest wall pressure fluctuations were observed in the location where the shear layer and vortices interacted with the wall. The analytical evaluation of sound source indicates that while bruits are connected with pressure fluctuations (as expressed in Eq. (11)), the sound detected by a stethoscope results from the integrated contributions from all locations in the lumen in the vicinity of the stenosis. This is confirmed by the present computational results, which show that the bruit spectrum coincides very well with the spectrum of the time-derivative of integrated pressure force. Furthermore, the analytically evaluated bruit spectrum agrees well with the computational result. Therefore, for the present canonical

configuration, it seems quite clear that the bruit sound is governed by the time-derivative of integrated pressure force on the wall of the blood vessel.

Having established that the bruit is associated with the fluctuating force on the vessel wall, the focus is turned towards determining the local region of the flow that is most responsible for the bruit sound generation. The most widely accepted notion in this context is that bruits are associated with the “disturbed” flow and the associated pressure fluctuation in the post-stenotic region. We investigated this issue by decomposing the total integrated pressure force and found that for the 50% constriction case, both the near and far post stenotic regions contribute equally to the bruit sound generation, but for 75% case, the bruit mostly originates from the near-post stenotic region. From these observations, we can conclude that the time-derivative of the integrated pressure force on the post-stenotic region is the dominant source of the bruit and this confirms the conjectures in some previous studies[8,13,24].

The present coupled hemodynamic-acoustic computational study enables us to establish that arterial bruits from stenosed arteries are directly related with the time-derivative of the integrated pressure force on the vessel wall, and that the most dominant contribution to this force comes from the post-stenotic pressure fluctuations that are caused by strong vortex motions and their interaction with the wall. Although the present study is limited to two-dimensional analysis, the source mechanism found in this study is not expected to change significantly for more realistic three-dimensional turbulent flows. Fredberg[12] has shown that the contribution of turbulence-associated wall pressure fluctuations is significantly diminished by the integration along the streamwise direction, especially for the higher frequencies associated with turbulence. The LES study of Mittal et al. [24] also found that the wall pressure fluctuations were strongest in the near-post stenotic region and were produced by the interaction of the shear layer with the wall. Taking all of this into consideration, it may be concluded that the contribution of turbulence to the bruit is very small and this supports the conjecture of Bruns[9] .

We also note that other effects such as those due to the viscoelastic nature of the arterial wall, shear wave propagation[31], and the presence of arterial branches[20] downstream of the stenosis are not considered. Despite these limitations, the current study provides a clear perspective on the generation of

bruits from stenosed arteries. Three dimensional effect and other mechanisms will be considered in a future study. The current approach is also being applied to the analysis of cardiac sounds including sounds associated with diastolic dysfunction[33] and systolic murmurs[27].

Acknowledgement

This research is partially supported by the CDI program at NSF through grant IOS-1124804. This work used the Extreme Science and Engineering Discovery Environment (XSEDE), which is supported by NSF grant number TG-CTS100002.

References

1. Ahmed SA, Giddens DP (1983) Velocity measurements in steady flow through axisymmetric stenoses at moderate Reynolds number, *J Biomech* 16: 505-516.
2. Ahmed SA, Giddens DP (1983) Flow disturbance measurements through a constricted tube at moderate Reynolds numbers. *J Biomech* 16:955-963.
3. Allen JB (1977) Short term spectral analysis, synthesis, and modification by discrete Fourier transform, *IEEE T Acoust Speech, ASSP-25(3)*: 235-238.
4. Ask P, Hok B, Lyold D, Terio H (1995) Bio-Acoustic signals from stenotic tube flow: state of the art and perspectives for future methodological development, *Med Biol Eng Comput* 33:669-675.
5. Banks H, Barnes J, Eberhardt A, Tran H, Wynne S (2002) Modeling and computation of propagating waves from coronary stenoses, *Comput Appl Math* 21: 767-788.
6. Baron C, Aubry J-F, Tanter M, Meairs S, Fink M (2009) Simulation of intracranial acoustic fields in clinical trials sonothrombolysis, *Ultrasound Med Biol* 35(7): 1148-1158.
7. Borisyuk AO (1999) Noise field in the human chest due to turbulent flow in large blood vessel, *Flow Turbul Combust* 61: 269-284.
8. Borisyuk AO (2002) Experimental study of noise produced by steady flow through a simulated vascular stenosis, *J Sound Vib* 256(3): 475-498.
9. Bruns DL (1959) A general theory of the causes of murmurs in the cardiovascular system. *Am J Med* 27(3):360-374.
10. Duncan GW, Gruber JO, Dewey CF, Meyers GS, Lees RS (1975) Evaluation of carotid stenosis by phonoangiography, *New Engl J Med* 293: 1124-1128.
11. Einstein DR, Kunzelman KS, Reinhall PG, Cochran RP, Nocosia MA (2004) Haemodynamic determinants of the mitral valve closure sound: a finite element study, *Med Biol Eng Comput* 42(6):832-846.

12. Fredberg JJ (1974) Pseudo-sound generation at atherosclerotic constrictions in arteries, *Bull Math Biol* 36:143-155.
13. Fredberg JJ (1977) Origin and character of vascular murmurs: model studies, *J Acoust Soc Am* 61:1077-1085.
14. Gaitonde D, Shang JS, Young JL (1999) Practical aspects of higher-order accurate finite volume schemes for wave propagation phenomena, *Int J Numer Method Eng* 45:1849-1869.
15. Goss SA, Frizzell LA, Dunn F (1979) Ultrasonic absorption and attenuation in mammalian tissues, *Ultrasound Med Biol* 5:181-186.
16. Goss SA, Frizzell LA, Dunn F (1980) Dependence of the ultrasonic properties of biological tissue on constituent proteins, *J Acoust Soc Am* 67(3):1041-1044.
17. Howe MS (1998) *Acoustics of Fluid-Structure Interactions*, Cambridge University Press, New York, pp 59-61.
18. Jones SA, Fronck A (1987) Analysis of break frequencies downstream of a constriction in a cylindrical tube, *J Biomech* 20:319-327.
19. Kirkeeide RL, Young DF, Cholvin NR (1977) Wall vibrations induced by flow through simulated stenoses in models and arteries, *J Biomech* 10(7):431-441.
20. Lee SW, Loth F, Royston TJ, Fischer PF, Bassiouny HS, Grogan JK (2005) Flow induced vein wall vibration in an arteriovenous graft, *J Fluid Struct* 20:837 - 852.
21. Lees RS, Dewey Jr C (1970) Phonoangiography: a new noninvasive diagnostic method for studying arterial disease, *P Natl Acad Sci* 67: 935-942.
22. Lele SK (1992) Compact finite difference schemes with spectral-like resolution, *J Comput Phys* 103:16-42.
23. Miller A, Lees RS, Kistler JP, Abbott WM (1980) Effects of surrounding tissue on the sound spectrum of arterial bruits in Vivo, *Stroke* 11: 394-398.
24. Mittal R, Simmons SP, Najjar F (2003) Numerical study of pulsatile flow in a constricted channel, *J Fluid Mech* 485:337-378.
25. Mittal R, Dong H, Bozkurtas M, Najjar FM, Vargas A, von Loebbecke AA (2008) A versatile sharp interface immersed boundary method for incompressible flows with complex boundaries, *J Comput Phys* 227:4825-4852.
26. Moon YJ, Seo JH, Bae YM, Roger M, Becker S (2010) A hybrid prediction method for low-subsonic turbulent flow noise, *Comput Fluids* 39:1125-1135.
27. Murgo JP (1998) Systolic ejection murmur in era of modern cardiology, what we really know? *J Am Coll Cardiol* 32(6):1596-1602.
28. Narasimhan C, Ward R, Kruse KL, Gudatti M, Mahinthakumar G (2004) A high resolution computer model for sound propagation in the human thorax based on the Visible Human data set, *Comput Biol Med* 34:177-192.
29. Nichols WW, O'Rourke MF (1998) *McDonald's Blood Flow in Arteries: Theoretical, Experimental, and Clinical Principles*, 4th Ed. Oxford University Press, New York, pp 37-38, 396-401.
30. Okita K, Ono K, Takagi S, Matsumoto Y (2010) Development of high intensity focused ultrasound simulator for large-scale computing, *Int J Numer Meth Fluids* 65:43-66.

31. Owsley NL, Hull AJ (1998) Beamformed nearfield imaging of a simulated coronary artery containing a stenosis, *IEEE T Med Imaging* 17: 900-909.
32. Pedley TJ (1980) *The fluid mechanics of large blood vessels*, Cambridge University Press, New York, pp 30.
33. Ronan JA Jr (1992) Cardiac auscultation: the third and fourth heart sounds, *Heart Dis Stroke* Sep-Oct;1(5):267-270.
34. Semmlow J, Rahalkar K (2007) Acoustic detection of coronary artery disease, *Annu Rev Biomed Eng* 9:449-469.
35. Seo JH, Moon YJ (2006) Linearized perturbed compressible equations for low Mach number aeroacoustics, *J Comput Phys* 218:702-719.
36. Seo JH, Mittal R (2011) A high-order immersed boundary method for acoustic wave scattering and low Mach number flow induced sound in complex geometries, *J Comput Phys* 230:1000-1019.
37. Varghese SS, Frankel SH, Fischer PF (2007) Direct numerical simulation of stenotic flows. Part 1. Steady flow, *J Fluid Mech* 582:253-280.
38. Varghese SS, Frankel SH, Fischer PF (2007) Direct numerical simulation of stenotic flows. Part 2. Pulsatile flow, *J Fluid Mech* 582:281-318.
39. Wang J, Tie B, Welkowitz W, Semmlow J, Kotis J (1990) Modeling sound generation in stenosed coronary arteries, *IEEE T Biomed Eng* 37:1087-1094.
40. Yazicioglu Y, Royston TJ, Spohnholtz T, Martin B, Loth F, Bassiouny H (2005) Acoustic radiation from a fluid-filled, subsurface vascular tube with internal turbulent flow due to a constriction, *J Acoust Soc Am* 118 (2):1193 - 1209.